



Detecting and Assessing the Spatio-Temporal Land Use Land Cover Changes of Bahrain Island During 1986–2020 Using Remote Sensing and GIS

Sabah S. Aljenaid¹  · Ghadeer R. Kadhem¹ · Manaf F. AlKhuzaei² · Jobair B. Alam³

Received: 26 October 2021 / Revised: 21 April 2022 / Accepted: 22 April 2022 / Published online: 16 May 2022
© The Author(s) 2022

Abstract

The Kingdom of Bahrain has experienced accelerated development growth since the 1980s. These rapid land demands increased the pressure on the country area to rebuild urban centers and cities surrounding the coast. The purpose of this research is to detect and investigate changes in land use and land cover (LULC), which is one of the most critical aspects of planning and managing the use of land as a natural resource. The massive growth in land demand, particularly in small-area countries like Bahrain, forces decision-makers to re-plan the main island areas (Bahrain, Muharraq, Sitra, and Nabih Saleh). The study focuses on mapping the LULC changes detection over 1986–2020. It employs an integrated approach of remote sensing and GIS (Geographic Information System) to analyze and evaluate the changes in the LULC area in the main islands using multi-temporal and multispectral Landsat satellite imagery acquired in 1986, 1994, 2000, 2005, 2013, and 2020. In addition, high-resolution satellite images of different dates IKONOS 2000, GeoEye1 2011, 2013, Worldview3 2019, ASTER 2012, 2013, and multiresolution seamless image database-MrSID 1994, 1998 were used to enhance the LULC classification. Furthermore, different ancillary data were utilized to adjust the decision of LULC classes. The images were supervised using Maximum Likelihood Classifier (MLC) algorithms to generate the seven LULC maps. The seven-raster classification maps revealed overall accuracies exceeding 85%, and overall Kappa statistics range between 87 and 95%. The results indicate that the increment in the built-up area was dominant over the last 3 decades.

Keywords Remote sensing · GIS · Land use land cover · Change detection · Chord diagrams · Bahrain

1 Introduction

The Kingdom of Bahrain's rapid development boom during the 1980s raised the demand for land, particularly in coastal areas, over the past 34 years (1986–2020). As a result, the pressure on the country's overall area to develop urban centers and re-design the existing cities along the shore had intensified due to this growing land demand. Therefore, different information and statistics on LULC are required for sustainable land resource management and policymaking processes to monitor continually, model, and update changes.

Remote sensing science and techniques play an essential role in producing spatial information and detailed raw data on terrestrial phenomena using space-borne platforms (Jansen and Gregorio 2004). These data on different geographical locations facilitate the characterization and evaluation of the changes (Yuan et al. 2005). Remote sensing data's spatial, temporal, and spectral characteristics are

✉ Sabah S. Aljenaid
Sabah@agu.edu.bh

Ghadeer R. Kadhem
ghadeermrk@agu.edu.bh

Manaf F. AlKhuzaei
mkhuzaei94@gmail.com

Jobair B. Alam
Jobair.Alam@houstontx.gov

¹ Department of Geoinformatics, College of Postgraduate Studies, Arabian Gulf University, PO. Box 2766, Manama, Bahrain

² School of Environment and Technology, University of Brighton, Brighton, UK

³ IMS Engineers, Houston, TX, USA

utilized to map LULC to aid in land resource management decision-making (Berlanga-Robles and Ruiz-Luna 2002). The emergence of satellite imagery has developed tools for systematic observation of land cover from space (Mollicone et al. 2003). Data required for large land areas are collected at different time intervals and used to monitor changes on the earth's surface (Jensen 2005). Landsat data help assess LULC for different years, analyze changes, understand land-use patterns and factors, and build databases for long-term monitoring tools when combined with geographic information system data and various statistical analytical tools (Jensen 2005). GIS and Remote sensings are effective techniques for obtaining precise and timely data and information on the spatial distribution of LULC changes over broad areas (Guerschman et al. 2003; Rogan and Chen 2004; Zsuzsanna et al. 2005). Remote sensing and GIS data have been used to map land uses and land cover and detect changes in many studies over the past fifty years. These data have been used to study expansion and urbanization, quantify land changes, and study the effects of land changes in faster, straightforward ways than traditional methods in survey studies (Da Costa and Cintra 1999). GIS provides a versatile framework for gathering, storing, displaying, and evaluating digital data needed for change detection (Demers 2008; Wu et al. 2006). GIS relies heavily on remote sensing imagery as a data source. Satellite imagery is employed to recognize synoptic data of the earth's surface (Ulbricht and Heckendorff 1998). Over the last 20 years, researchers concentrated on using remotely sensed image band characterization to study urban and nonurban area changes (Gadal and Ouerghemmi 2019; Vigneshwaran and Kumar 2018; Jacquin et al. 2008; Xu 2007; Zha et al. 2003). Due to their ability to provide immediate and synoptic usage of land cover, remotely sensed images are suitable tools for identifying, managing, and monitoring urban built-up areas, spatial distribution, and expansion (Hegazy and Kaloop 2015; Rawat and Kumar 2015). Many types of research used different classification techniques such as supervised, unsupervised, object-based, or deep learning classification in their studies for extracting urban areas from a multispectral satellite image (Ghosh and Siddique 2018; Bramhe et al. 2018; Forget et al. 2017; Hegazy and Kaloop 2015; Rawat and Kumar 2015; Zhang et al. 2014; Ndehedehe et al. 2013). With a spatial accuracy of 30 m, Landsat multispectral images became the backbone of large-scale land cover change studies due to the long period covered by satellite data over 45 years (Duan et al. 2020; Tewabe and Fentahun 2020; Lu et al. 2010; Wulder et al. 2008; Cohen and Goward 2004). Many satellite images are being used to monitor and study land cover changes, such as SPOT, ASTER, IR, IKONOS, QuickBird, WorldView1, 2, 3 (Allen et al. 2013; Lu and Weng 2009). The land cover information extracted from remote sensing data is an essential part of various applications, including land-use mapping

and monitoring of variables. Different satellite-based LC data applications have been created in the last 30 years. The most important of which is the analysis of land cover dynamics that significantly impacts natural habitats (Yuan et al. 2005), as well as the creation of LC maps utilizing a variety of classification methods, all of which are linked to direct statistics to determine classification accuracy and error ratio. Land cover analysis and classification results are based on four main characteristics: temporal, spatial, radiometric, and spectral accuracy (Allen et al. 2013). Macleod and Congalton (1998) identified four manifestations of detection of land-use changes in the study of land resources, namely, the detection of changes that have occurred, the determination of nature of change, the measurement of the areal extent of change, and the assessment of the spatial pattern of change (Macleod and Congalton 1998). Landsat Multispectral Scanner (MSS), Thematic Mapper (TM), and Enhanced Thematic Mapper Plus (ETM+) data have been broadly employed in studies towards the determination of land cover since 1972, the starting year of the Landsat program, mainly in forest and agricultural areas (Campbell 2007). The availability of detailed data on land uses for urbanization is essential for planning processes (Jensen and Cowen 1999). Remote sensing data have become the cornerstone of all urban studies emphasizing mapping and analyzing the changes in area, extent, and patterns (Wang et al. 2020). Open access to earth observation satellite data provides spatially valid datasets over broad areas with great spatial detail and temporal frequency (Xiao et al. 2006). The availability of many free satellite images and GIS layers and improvements in remote-sensing data gathering with increased spatial accuracy allow and improve quantitative studies of the rate and pattern of urban LULC change (Epstein et al. 2002).

2 Study Area

The Kingdom of Bahrain is an archipelago of 36 low-lying islands that vary in size, surrounded by shallow waters no deeper than 20 m. The country is located in the southern part of the Arabian Gulf. Its territorial water covers roughly 9200 km² and accounts for more than 90% of the total area. In 2015, the country's land area was estimated to be 782.4 km² (2020), including rocky coral atolls (Fashts), as shown in Fig. 1. The coastal length is more than 537 km, and the marine area is more than 9200 km (Information and eGovernment Authority 2020). The country has significant population and infrastructure growth, which has raised the demand for land (UNDP 2018). As a result, the country's land area has increased from 697 km² in 1987 to 782 km² in 2019 (Information and eGovernment Authority 2020). Due to the increased demand for land, the increment rate reached its maximum

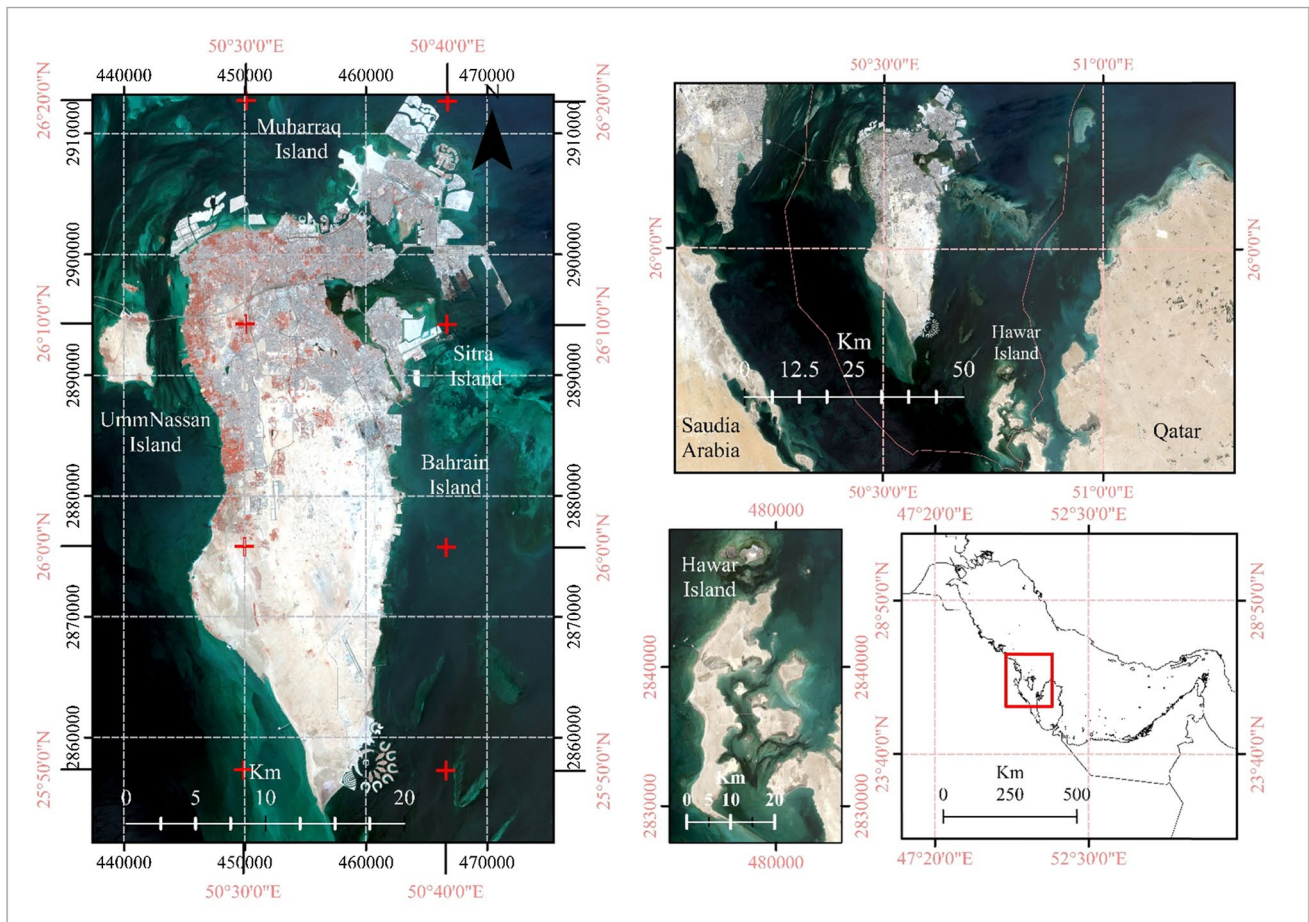


Fig. 1 The Kingdom of Bahrain Islands location between Saudi Arabia and Qatar in the Arabian Gulf. This (Satellite Image map download from <https://earthexplorer.usgs.gov/>, then Mosaic. ID: LIC_T39RVJ_A030419_20210419T071115, Acquisition Date:

2021/04/19, Platform: SENTINEL-2A, Tile Number: T39RVJ.AND, ID: LIC_T39RVK_A030419_20210419T071115, Acquisition Date: 2021/04/19, Platform: SENTINEL-2A, Tile Number: T39RVK)

point (21 km²/year) between 1997 and 2007 (UNDP 2018). The majority of the country’s population (more than 95%) lives in densely populated coastal areas (Mesaiqer and Al-Zayani 2008). From the 1950s until 2007, the population increased by 2.7 percent per year, reaching around 435,654 in 1987 and over 544,366 in 1994. In 2013, the estimated population was 1,253,191, which was expected to grow to 1,523,084 by 2020 (CIO (1986–2013); Information and eGovernment Authority 2020). According to CIO’s (1986–2013) predictions, the country’s population will reach 2.2 million by 2030 (Information and eGovernment Authority 2018; UNDP 2018). Increased demand for land, notably for urbanization and creating new cities and residential facilities, has increased population. More than half of Bahrain’s main island is almost entirely urbanized. Aside from considerable pressure on infrastructure, health, education, and social services, the country is vulnerable to some issues due to its arid desert climate and small land area (UNDP 2018; UNdata 2021).

3 Methodology

3.1 Data Acquisition

In this analysis, we used 30 m dry season six Landsat cloud-free datasets: Landsat-5, Thematic Mapper (TM) from August 14, 1986, Landsat-7 from July 11, 2000, Enhanced Thematic Mapper Plus (ETM+) from July 25, 2005, and Landsat-8 Operational Land Imager (OLI) from August 24, 2013, and August 11, 2020. Table 1 shows the specifics of Landsat satellite image data downloaded from the Earth Explorer website of the United States Geological Survey (USGS) (<https://earthexplorer.usgs.gov/>). Earth Explorer is an online website that allows searching, viewing, exporting information, and downloading earth science data from the USGS (EROS 2021). In addition, the images were spatially registered on the World Geodetic System (WGS84) and then re-projected the data to the Northern Hampshire zone 39N on Universal Transverse Mercator (UTM) projection. We

Table 1 Details of Landsat Band data used for this study collected from EarthExplorer

Year	Satellite/sensor	Date of acquisition	Sensor	Land cloud cover (%)	Resolution (m)	Wavelength (μm)
2020	Landsat 8 OLI	11-08-2020	Operational Land Imager (OLI)	0.3	30 m	Band 1: 0.435–0.451
2013		24-08-2013		0		Band 2: 0.452–0.512
						Band 3: 0.533–0.590
						Band 4: 0.636–0.673
						Band 5: 0.851–0.879
						Band 6: 1.566–1.651
						Band 7: 2.107–2.294
2005	Landsat 7 ETM+	25-07-2005	Enhanced Thematic Mapper Plus (ETM+)	0		Band 1: 0.45–0.52
2000		11-07-2000		0		Band 2: 0.52–0.60
1994	Landsat 5 TM	20-08-1994	Thematic Mapper (TM)	0		Band 3: 0.63–0.69
1986		14-08-1986		0		Band 4: 0.76–0.90
						Band 5: 1.55–1.75
						Band 7: 2.09–2.35

used the Maximum Likelihood Classifier (MLC) algorithms to classify the images. All the maps were assigned to the WGS 1984 UTM Global Geodetic Coordinates System. We used the 2020 Landsat 8 OLI image as the master reference for all the images and data used in this study.

3.2 Ancillary Data

Ancillary data, also known as auxiliary data, are frequently utilized to improve image classification and accuracy. Due to the limitations of spectral information for defining change, researchers must rely on auxiliary data (Franklin 1995). To determine LULC Changes processes, many researchers used ancillary data as input features with multi-temporal images (Hurskainen et al. 2019; Feng et al. 2018; Zhu et al. 2016; Zoungrana et al. 2015; Yu et al. 2013). This study used high-resolution satellite images for different dates: IKONOS 2000, GeoEye1 2011, 2013, Worldview3 2019, and the multiresolution seamless image database-MrSID

1994, 1998, and ASTER 2012, 2013 to enhance the LULC-classification. We used auxiliary data, mainly Bahrain topographic scanned maps from the “Survey and Land Registration Bureau (SLRB)” scale 1: 50,000, 25,000, and 10,000, to adjust the decision of LULC-classes, Fig. 2. In addition, we assimilated the four digital governorates zoning maps; Capital, Muharraq, Northern, and Southern (UPDA 2022) that published by the general directorate of urban planning at the “Urban Planning and Development Authority” <https://upda.gov.bh/> to validate the classification results (Harris and Ventura 1995).

3.3 LULC Classes Definition

The classification of LULC is based mainly on its creation, with the levels being divided into numerous levels based on the level of accuracy and purpose necessary. We adapted the LULC level-1 classification from Anderson et al. (1976). Most of these categories were based on statistical data, aerial

Fig. 2 Ancillary data: **a** IKONOS 2000, **b** MRSID 1994, **c** Bahrain Zoning Map, 2017, and **d** topographic map 1:25,000 of the same area from 1986



photos, satellite imagery data, or directly based on Anderson et al. (1976) or other land classifications. We created a classification scheme for this study based on prior knowledge of the study region and information derived from auxiliary data and information (Anderson et al. 1976). The accessible digital Bahrain Zoning maps (UPDA 2022) and other auxiliary data were the primary sources for identifying the research area’s main LULC classes. As a result, seven LULC classes covering the surface study area were identified and classified, including the reclaimed area (Rec), vegetation (Veg), built-up/urban area (Bul), rock outcrop (Roc), bare ground (Bar), gypsic soil (Gyp), and wetland/sabkhas region (Wetland/Sabkhas) (Wet). Table 2 displays the seven LULC classification schemes adapted for this study.

3.4 Image Preprocessing

This study used multitemporal and multispectral Landsat satellite images acquired in 1986, 1994, 2000, 2005, 2013, and 2020. The changes in the LULC areas were detected using a Supervised Maximum Likelihood Classification algorithm for the six temporal dates. Remote sensing and GIS Software were used to handle the geometric and radiometric enhancement, mosaicking, and the sub-setting of Landsat 5 Thematic Mapper (TM), Landsat 7, Enhanced Thematic Mapper Plus (ETM+), and Landsat 8 Operational Land Imager (OLI) images. Furthermore, high-resolution satellite images of different dates IKONOS, 2000, GeoEye1 2011, 2013, Worldview3, 2019, ASTER, 2012, 2013 and multiresolution seamless image database-MrSID 1994, 1998 were used to enhance the LULC-classification. Image-preprocessing operations for this study include geometric correction (rectification), ETM+ Scan Line Corrector–SLC off and gap filling, radiometric, and atmospheric calibration (Lu et al. 2004). Geometric (rectification), ETM+ Scan Line Corrector–SLC off and gap filling, radiometric, and

atmospheric calibration are a few of the image-preprocessing techniques used in this study (Lu et al. 2004). All the images were co-registered and radiometrically calibrated to compare different temporal dates of the study area. Radiometric calibration was done to reduce or correct errors in the digital numbers of the images. The calibrated Digital Numbers (DNs) were first transformed to absolute units of at-sensor spectral brightness and then to Top-Of-Atmosphere (TOA) reflectance (Chander et al. 2009). The DNs stored in the original image are converted into biophysical variables of standard significance (reflectance). For Landsat 5, 7, and 8, the TOA spectral radiance is calculated using the band-specific multiplicative rescaling factor. The TOA reflectance is then adjusted for the solar angle. TOA reflectance has three advantages over at-sensor spectral radiance when comparing images from different sensors. First, the time difference between data collection reduces the cosine effect of differing solar zenith angles. Second, TOA reflectance adjusts for spectral band changes in exo-atmospheric solar irradiance, resulting in varied values of exo-atmospheric solar irradiance. Third, the TOA reflectance compensates for differences in Earth–Sun distance between data gathering dates. These variances might be significant geographically and temporally (Chander et al. 2009).

3.5 Image Classification

We employed the supervised classification methodology to classify the LULC categories (sites) into the predetermined seven classes in this study, Table 2. Combining training samples (sites) with prior knowledge and familiarity with the study area is necessary to complete the supervised classification (Jensen 2005). The training sites were chosen based on visible areas in all the image sources. We began by defining polygons around representative portions of each LULC category (Sites) in each Landsat image as identified and defined

Table 2 Definitions of LULC classes (Source: modified partially from Anderson, 1976)

LULC classes	Code	Description
Reclaimed	Rec	Areas with a natural or artificial cover because of dredging and reclamation mainly surround the coast. In addition, it includes the drilled and backfills with marine sand. It has been used for construction purposes after that
Vegetation	Veg	It comprises an area covered by various plants, whether seasonal or permanent, scattered trees, and palm trees
Built-up/urban area	Bul	Areas include heavily used areas covered by constructions. These include cities, municipalities, villages, and developed areas adjacent to public roads, transportation, electricity, communications and infrastructure, shopping centers, commercial and industrial parks, institutions, and other constructions relevant to non-agricultural human industries
Rock outcrop	Roc	Fragmented carbonate and dolomitic carbonate rocks dominate Bahrain’s structural Dome outcrop
Bare land	Bar	Areas with exposed soils and un-vegetated land generally contain thin soil, bare soil, sand, or rocks
Gypsic soil	Gyp	Areas covered with Gypsisols soil are a fine white powder, crystals, pebbles, and stones formed through dissolution from calcium sulfate
Wetlands/sabkhas	Wet	In-land and near shallow coasts, marshes, mudflats, natural sabkhas, and the in-land are formed by dredging and filling

in Table 2. Between 200 and 500 training sites were identified in each rectified satellite image. We employed the maximum likelihood classifier-MLC to produce spectral signatures to classify all the pixels in the image after the training sites had been established. Following the first classification, a majority filter was used to smooth the classification results by reducing noise from the classed raster maps, resulting in the final LULC raster maps utilized for further analysis. The 1:10,000 Bahrain topographic maps were utilized to construct ground signatures for the supervised categorization of the 1986 image. For the 1994 supervised classification, ground control signatures were created using MrSID orthophotos from 1994 and Bahrain topographic maps at a scale of 1:10,000. The ground signature was created for the 2000 Landsat ETM image using high-resolution IKONOS 2000. The Landsat 2005 ETM image and the Landsat 2013 OLI image, ASTER 2005 and 2013, were utilized to construct ground signatures. Ground signatures for the Landsat 2020 OLI were created utilizing Sentinel 2. The six images were classified into seven classes, namely built-up/urban area (Bul), bare land (Bar), gypsic soil (Gyp), reclaimed land (Rec), rock outcrop (Roc), vegetation (Veg) and wetlands/sabkhas (Wet) as displayed in Table 2. We then supervised all the images using the maximum MLC algorithm (Lillesand and Kiefer 1999).

3.6 Accuracy Assessment

The error matrix is the most used technique for determining accuracy (Congalton and Green 2019). The classification accuracy can be evaluated to produce an overall measure of the map's quality, which can then be used to compare alternative change detection systems (Foody 2002). The minimum level of accuracy in interpreting remote sensing data to identify LULC classes should be at least 85% (Anderson et al. 1976). These standards error matrices (accuracy assessment statistics) are computed based on the same data references for each image to calculate the components of overall accuracy, user's accuracy, producer's accuracy, error of commission (EC), error of omission (EO), and kappa coefficient. Overall accuracy (OA) is the total number of successes compared to the total number of samples in the categorized image. It is calculated by summing the number of correctly classified values and dividing it by the total number of values in the confusion matrix in Eq. (1). User's accuracy (UA) is the probability of classified pixel on each map representing the actual class on the ground or real-world location (Congalton 1991; Jensen 2005; Campbell 2007) and is calculated using Eq. (2). On the other hand, the producer's accuracy (PA) measures the error of omission. It is the probability that a reference pixel is classified correctly. It is calculated by dividing the number of corrected classified samples

of a specific category by the total number of reference samples using Eq. (3). The error of commission (EC) is the proportion of a pixel that is predicted to be in a class, but it does not. It is calculated using Eq. (4). The error of omission (EO) is the proportion of observed pixels on the ground that are not classified on the map, and it corresponds to the producer's accuracy. The kappa coefficient (KC) is a measure of the difference between the actual agreement between reference data and an automated classifier and the chance agreement between the reference data and a random classifier, expressed using Eq. (5) (Lillesand et al. 2015). The percentage of correctly categorized pixels is calculated from the percentage expected by chance. It measures the difference between the actual agreement and chance (random) agreement between the map and the validation data on the ground (Congalton 2001). The higher the classification accuracy of the map, the more valuable it is for land administrators and land-use planners. The KC (Koc et al. 2012) is a discrete multivariate approach for determining the level of agreement or accuracy. Its value ranges from -1 to 1 . However, it frequently falls between 0 and 1 (Zanotta 2018):

Overall Accuracy (OA)

$$= \frac{\text{Sum of diagonal (correctly identified)}}{\text{Total number of samples}} \times 100 \quad (1)$$

User's Accuracy (UA)

$$= \frac{\text{Samples correctly identified in the row}}{\text{Row total}} \times 100 \quad (2)$$

Producer's Accuracy (PA)

$$= \frac{\text{Samples correctly identified in the column}}{\text{Column total}} \times 100 \quad (3)$$

$$\text{Error of Omission (EO)} = \frac{\sum \text{off Diagonal element of Column}}{\text{Column Total}} \times 100 \quad (4)$$

$$\text{Kappa Coefficient (KC)} = \frac{N \sum_{i=1}^r x_{ii} - \sum_{i=1}^r (x_{i+} \times x_{+i})}{N^2 - \sum_{i=1}^r (x_{i+} \times x_{+i})} \quad (5)$$

where r is the rows number in the matrix, x_{ii} is the number of observations in row i and column i (the diagonal elements), x_{+i} and x_{i+} are the marginal totals of row i and column j , respectively, and N is the observations' number.

This study used the error matrix (confusion matrix), the most efficient accuracy assessment method for the six-time period's MLC raster classified maps: 1986, 1994, 2000, 2005, 2013, and 2020 (Roy and Inamdar 2019). We used this step to quantitatively assess how efficiently the classified remotely sensed data pixels were sampled into corrected LULC's category. The resulting classified images

were verified pixel by pixel for the accuracy assessment (Keshtkar et al. 2017). The seven classes, Table 2, were considered for accuracy assessment with a minimum of 71 sample points for each defined class, as recommended by Congalton (1991). We used the “Equalized stratified random” sampling method to create randomly distributed points, where each class has the same number of points. Four hundred and ninety-seven (497) systematic point samples for each classified image were used to test the precision by comparing them with specific points from the available ancillary data for this study. We calculated the confusion error matrix considering an accuracy level equal to or above 85% to be an excellent and reliable LULC classification as recommended by previous studies (Alrababah and Alhamad 2006; Manandhar et al. 2009; Koc et al. 2012). We used the confusion matrix for obtaining descriptive and analytical statistics of the classification accuracy assessment, as explained in Sup Tables 1–6 (Foody, 2002; Congalton, 1991; Jensen, 2005).

3.7 Change Detection

Change detection aims to compare the spatial representation of two points in time while controlling all variations due to differences in the variables of interest (Green et al. 1994). The ability to identify changes in the earth’s surface features in real-time and with high accuracy lays the groundwork for a greater understanding of the linkages and interactions between human and natural events, allowing for improved resource management and use (Lu et al. 2004). The most common data type used to detect changes is geographic data, usually in digital forms such as satellite imagery, analog format (earlier aerial images), and vector format (maps). Other data types, such as historical and economic data, can be employed (Singh 1989). Due to the availability of massive archival data sets in recent decades, several digital change detection algorithms and methodologies for evaluating and identifying LULC changes have been developed and evaluated (Dewidar 2004). These methods and procedures have been thoroughly examined, with great descriptions and summaries supplied (Haque and Basak 2017). Since digital change detection is significantly influenced by the temporal, spatial, spectral, and thematic resolutions of remotely sensed data, choosing the right change detection approach is critical for producing accurate findings (Lu et al. 2004). Image differencing, image rationing, PCA, CVA, and Post-Classification Comparison are the most common approaches for detecting changes (Xu et al. 2009; Bekalo 2009). The use of machine-learning techniques on remotely sensed imageries has recently received a lot of consideration (Maxwell et al. 2018; Adam et al. 2014). LULC classification applications have used different machine-learning advanced methods. For the supervised classification techniques, many researchers

used support vector machine (SVM), spectral angle mapper (SAM), Mahalanobis distance (MD), random forest (RF), fuzzy adaptive resonance theory-supervised predictive mapping (Fuzzy ARTMAP), radial basis function (RBF), decision tree (DT), multilayer perception (MLP), naive Bayes (NB), maximum likelihood classifier (MLC), and fuzzy logic (Ma et al. 2019; Shih et al. 2019). The Affinity Propagation (AP) cluster method, fuzzy c-means algorithms, K-means algorithms, and ISODATA are examples of unsupervised classification approaches (iterative self-organizing data) (Maxwell et al. 2018; Camps-Valls et al. 2011). As a result, multiple studies on LULC modeling have been conducted utilizing various machine-learning techniques (Talukdar et al. 2020) and comparing machine-learning algorithms (Camargo et al. 2019). In addition, some research has been conducted to determine the most appropriate and accurate algorithm for LULC mapping among the many machine-learning classifiers (Camargo et al. 2019; Jamali 2019). In this study, we used the GIS-based change detection approach, which integrates GIS and remote sensing method (Lu et al. 2004) to explore and identify the changes that have taken place to the spatial extent and pattern of our study area (Gallego 2004). We used GIS because of its ability to incorporate a different source of data with different data accuracies and formats (Petit and Lambin 2001) for long-period intervals into LULC change detection (Lu et al. 2004). This approach helps analyze the direction, rate, and spatial pattern of LULC changes (Weng 2002). The magnitude of change (MC), the percentage of change (PC), and the annual rate of change (ARC) of the classified images were calculated based on the following equations:

$$MC(km^2) = A_i - A_f \tag{6}$$

$$PC(\%) = \frac{A_i - A_f}{A_i} \times 100 \tag{7}$$

$$ARC(km^2\text{year}^{-1}) = \frac{A_i - A_f}{n} \tag{8}$$

$$ARC(\%) = \frac{A_i - A_f}{A_i \times n} \times 100 \tag{9}$$

where A_i is the class area (km^2) at the initial time, A_f is the class area (km^2) at the final time, and (n) is the number of years of the study period.

There are different techniques for change detection analysis, and the most common and used ones include post-classification comparison, image ratio, and manual on-screen digitization of change, principal components analysis, image regression, conventional image differentiation, and multi-date image classification (Ayele et al. 2018; Lu et al. 2004).

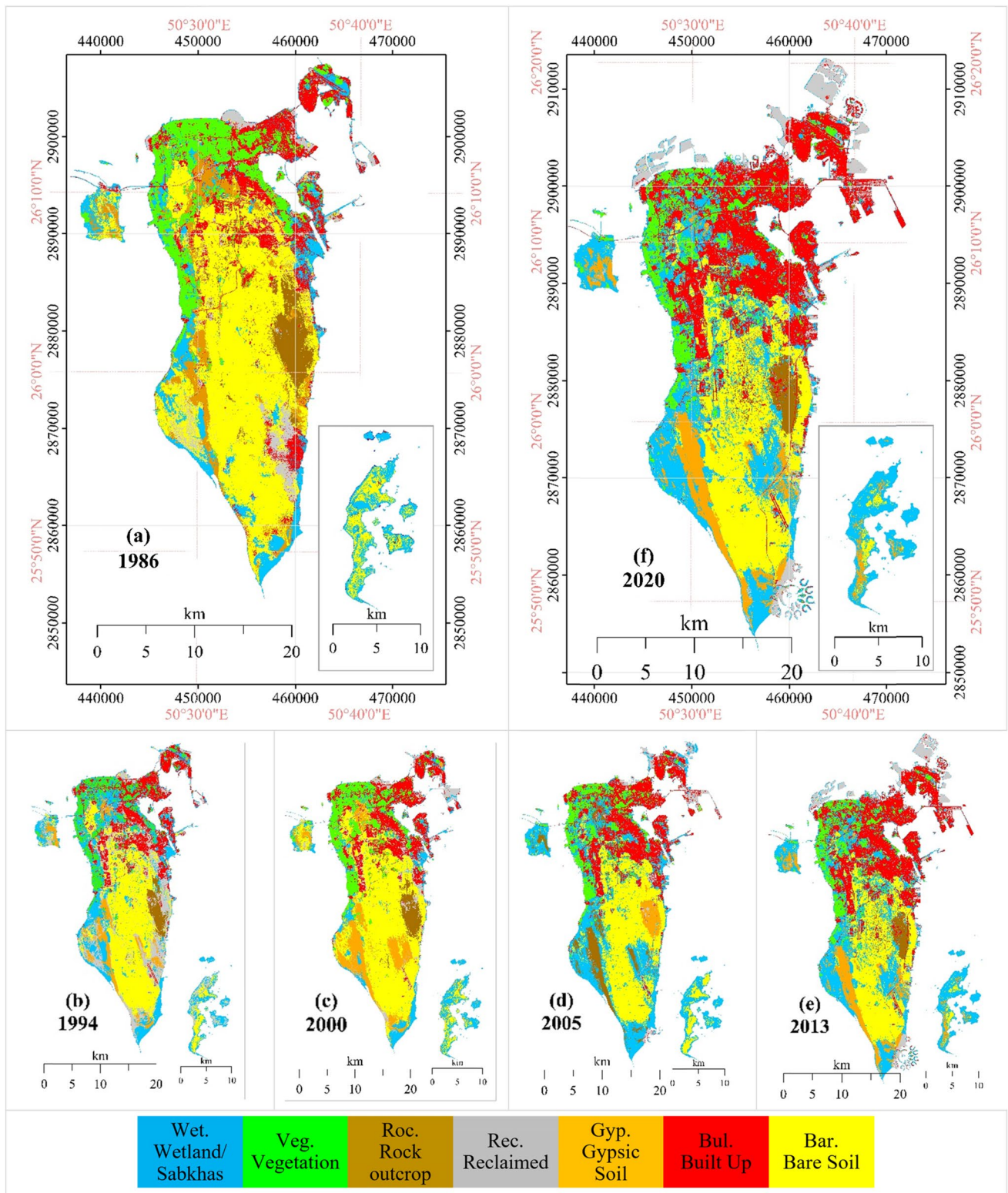


Fig. 3 Land Use Land Cover (LULC) classes for **a** 1986, **b** 1994, **c** 2000, **d** 2005, **e** 2013 and **f** 2020

Table 3 LULC area by class and its percentage to the total area (km²) 1986–2020

Class	1986		1994		2000		2005		2013		2020	
	Total area in km ² and %											
	Area	%	Area	%	Area	%	Area	%	Area	%	Area	%
Reclaimed	41.6	6.0	131.4	18.6	54.2	7.6	34.9	4.8	52.8	6.9	64.1	8.2
Vegetation	78.4	11.2	55.4	7.8	83.2	11.6	64.6	8.8	62.2	8.1	54.4	6.9
Built-up	87.7	12.6	102.5	14.5	112.1	15.6	143.2	19.6	190.9	24.8	312.2	39.8
Rock outcrop	33.0	4.7	19.0	2.7	24.3	3.4	17.6	2.4	21.8	2.8	18.9	2.4
Bare soil	288.9	41.4	205.4	29.1	266.5	37.2	208.1	28.4	163.7	21.2	301.1	38.4
Gypsic soil	57.8	8.3	38.6	5.5	81.8	11.4	42.9	5.9	58.6	7.6	6.3	0.8
Wetland/sabkhas	110.8	15.9	154.6	21.9	94.7	13.2	220.7	30.2	220.8	28.6	27.3	3.5
Total	698.2	100	706.8	100	716.8	100	731.9	100	770.9	100	784.4	100

Table 4 LULC classes in 1986, 2005, and 2020 and the spatio-temporal changes of the study area

LULC classes	1986	2005	2020	Change 1986–2005		Change 2005–2020		Change 1986–2020		Annual rate of change 1986–2020	
	Area (km ²)			Area (km ²)		Area (km ²)		Area (km ²)		Area (km ²)	
				Area (km ²)	%	Area (km ²)	%	Area (km ²)	%	Area (km ²)	%
Reclaimed	41.60	34.9	64.1	−6.66	16.01	29.2	83.67	22.54	35.16	0.66	−1.59
Vegetation	78.38	64.6	54.4	−13.76	17.56	−10.17	15.74	−23.93	43.99	−0.70	−0.90
Built-up	88.00	143.2	312.2	55.5	63.07	169.05	118.05	224.54	71.92	6.60	7.49
Rock outcrop	33.00	17.6	18.9	−15.47	46.88	1.36	7.73	−14.11	74.66	−0.42	−1.26
Bare soil	289.00	208.1	301.1	−80.84	27.97	93.05	44.71	12.22	4.06	0.36	0.12
Gypsic soil	57.80	42.9	6.3	−14.9	25.78	−36.6	85.31	−51.5	817.46	−1.51	−2.62
Wetland/sabkhas	110.80	220.7	27.3	109.99	99.27	−193.4	87.63	−83.41	305.53	−2.45	−2.22
Total area	698.20	731.9	784.4	−	−	−	−	−	−	−	−

We used the post-classification comparison techniques to integrate the six classified images, which were classified individually to produce a land cover raster map, Fig. 3a–f, Tables 3 and 4. Then, we compared the corresponding classes to identify areas where change has occurred (El-Hattab 2016). We build a series of “from-to” matrixes by comparing them on a pixel-by-pixel basis (Jensen 2005; Aldoski et al. 2013). It involves the overlay (or “stacking”) of two or more classified images. Change areas are simply those not classified the same at different times. The multi-date change detection uses a binary mask applied to two dates (Jensen 1996; Dobson et al. 1995) and quantifies the change rates and magnitude (Ukor et al. 2016). The degree of change detection success depends on the accuracy of each image classification (Jensen 2005). Many researchers utilizing USGS-Landsat achieves data (Islam et al. 2018; Matlhodi et al. 2019; Tena et al. 2019; Butt et al. 2015; Rawat and Kumar 2015) to undertake post-classification technique-based MLC for detecting LULC changes. Pairs of the produced classified raster maps of the six dates (1986, 1994, 2000, 2005, 2013, and 2020) were compared by applying Boolean logical “AND” operation using GIS Software. Three matrixes were developed to understand

the changing status and magnitude rate for 1986 to 2005, 2005 to 2020, and 1986 to 2020, Table 5. In addition, six chord diagrams were created using Microsoft Power BI to visualize the classified raster maps classes (Fig. 4a–f), and three to visualize the changes in the specified temporal dates (Fig. 5a–c). In addition, the data presented in Table 5 was used to create three-chord diagrams to visualize the changes for the specified years in this study: 1986–2005, 2005–2020, and 1986–2020 (Fig. 5a–c). These diagrams represent the changes in the seven LULC-classes in the study area: reclamation, vegetation, built-up, rock outcrop, bare soil, Gypsic soil, and wetland from the “initial year” to the “first year.” The data in the three tables were reconstructed and added to the program to fit the parameters’ criteria. The Chord visual offers three fields (From, To, and Values). The data from the initial year go into the first field (From), the data from the first year (year of change) go into the second field (To), and the change between classes goes into the third field (Values). Finally, the Chord diagram is displayed according to the parameters selected visually (Data Visualization | Microsoft Power BI, n.d.; Ferrari and Russo 2016). Different researchers have employed Chord-Diagram, as a graphical approach for visualizing the inter-relationships between data

Table 5 LULC-classes change detection for 1986–2005, 2005–2020, and 1986–2020 (km²)

LULC classes	Period	Rec	Veg	Bul	Roc	Bar	Gyp	Wet
Reclamation (Rec)	1986–2005	−6.7	1.1	12.3	0.2	5.6	4.2	14.1
	2005–2020	29.2	0.7	25	0.2	1.8	0.1	0.4
	1986–2020	22.5	1.3	18.2	0.1	18	0.6	1.0
Vegetation (Veg)	1986–2005	0.5	−13.8	16.9	0.0	0.1	1.5	16.1
	2005–2020	0.5	−10.2	26.7	0.0	0.6	0.0	0.6
	1986–2020	1.0	−23.9	43.6	0.0	1.6	0.0	0.5
Built-up area (Bul)	1986–2005	3.4	6.4	55.5	0.1	3.8	1.8	11.8
	2005–2020	3.2	4.8	169	0.0	1.8	0.0	0.5
	1986–2020	2.0	4.1	241.7	0.0	9.0	0.2	0.7
Rock outcrop (Roc)	1986–2005	1.8	0.1	2.0	−15.5	11.9	0.4	1.9
	2005–2020	2.1	0.0	6.3	1.4	2.8	0.0	0.0
	1986–2020	3.8	0.2	12.3	−14.1	7.5	0.1	0.1
Bare soil area (Bar)	1986–2005	3.1	3.5	21.3	1.5	−80.8	12.3	78.9
	2005–2020	4.9	1.1	25.8	12	93.1	0.1	0.3
	1986–2020	6.5	5.4	60.8	9.3	12.2	1.6	3.1
Gypsic soil (Gyp)	1986–2005	1.7	4.4	7.5	0.5	6.3	−14.9	19.6
	2005–2020	2.1	0.8	7.6	0	25.8	−36.6	1.5
	1986–2020	3.7	4.5	23.9	0.4	20.4	−51.5	1.2
Wetland/sabkhas (Wet)	1986–2005	3.1	5.4	14.4	0.4	12.1	5.0	110.0
	2005–2020	14.6	9.5	64.9	0.4	102.5	0.8	−193.4
	1986–2020	8.4	5.5	35.4	0.0	40.3	0.1	−83.4

in building the transition matrices (e.g., Chen et al. 2017; Ferrara et al. 2021; Kacem et al. 2021; Xiao et al. 2021; Siddique et al. 2020; Vinatier and Arnaiz 2018; Viana and Rocha 2020).

4 Results and Discussion

4.1 Accuracy Assessment

We used six confusion matrices to assess the classification accuracy in this study. Sup Tables 1–6 indicate that the image classification achieved satisfying accuracy results. The OA of the classified images was 88.73, 89.54, 89.13, 88.93, 90.34, and 95.77% for the temporal dates 1986, 1994, 2000, 2005, 2013, and 2020, respectively, thus ascertaining that the classification was within the excellent range according to Anderson et al. (1976), as he indicated that the minimum accuracy value for reliable LC-classification is 85%. The KA reached 86.85, 87.79, 87.32, 87.09, 88.73, and 95.07% for 1986, 1994, 2000, 2005, 2013, and 2020, individually. The results of the seven classes for all the temporal times have excellent individual user's accuracy ranges between 80% and more than 94% for 1986. The user's accuracy for all the classes is outstanding except for the "Rock outcrop," about 80.28%, and "Gypsic soil," which is 81.69%. In 1994, the UA ranged from 73% to more than 97%, and the results indicate that the "Vegetated" surfaces

were most accurately classified (97.18). The less accurate class is "Reclaimed" land, 73.24%. In 2000, the UA ranged between 70 and 100%. The 2000 classified image results indicate that the "Vegetated" and "Rock outcrop" surfaces were most accurately classified (95.77%). The less accurate class is Gypsic, which is 83.1%. The 2005 classified image results indicate that the "Vegetation" surface revealed that UA reached 95.55%, while all the other classes of UA ranged between 83.1% and 87.32%. The UA of 2013 and 2020 Landsat8 OLI-classified images ranged between 91.55% and 98.59% and 87.32 and 100%, respectively. The producer's accuracy (PA) has a nearly excellent result for all class-classified images. In 1986, the PA ranged between 76.47 and 100%. In addition, the results indicate that the "Reclaimed area" surfaces were most accurately classified (100%). The less accurate class is "Bare Land" land, 76.47%. In 1994, the PA ranged between 68% and more than 98.39%. Furthermore, the results indicate that the "Gypsic soils" surfaces were most accurately classified (98.39). The less accurate class is the "Bare land" area, 68%. The 2000 classified image results indicate that the "Rock outcrop." Moreover, "Gypsic soils" surfaces were most accurately classified (100%). The less accurate class is the built-up area, which is 77.11%. The 2005 classified image results indicate that the "Gypsic soils" surface revealed a PA up to 96.72%, while all the other classes of PA ranged between 77.78 and 95.24%. The UA of 2013 and 2020 Landsat8 OLI-classified images ranged between 93.15 and 100% and 92.65 and 100%, respectively.

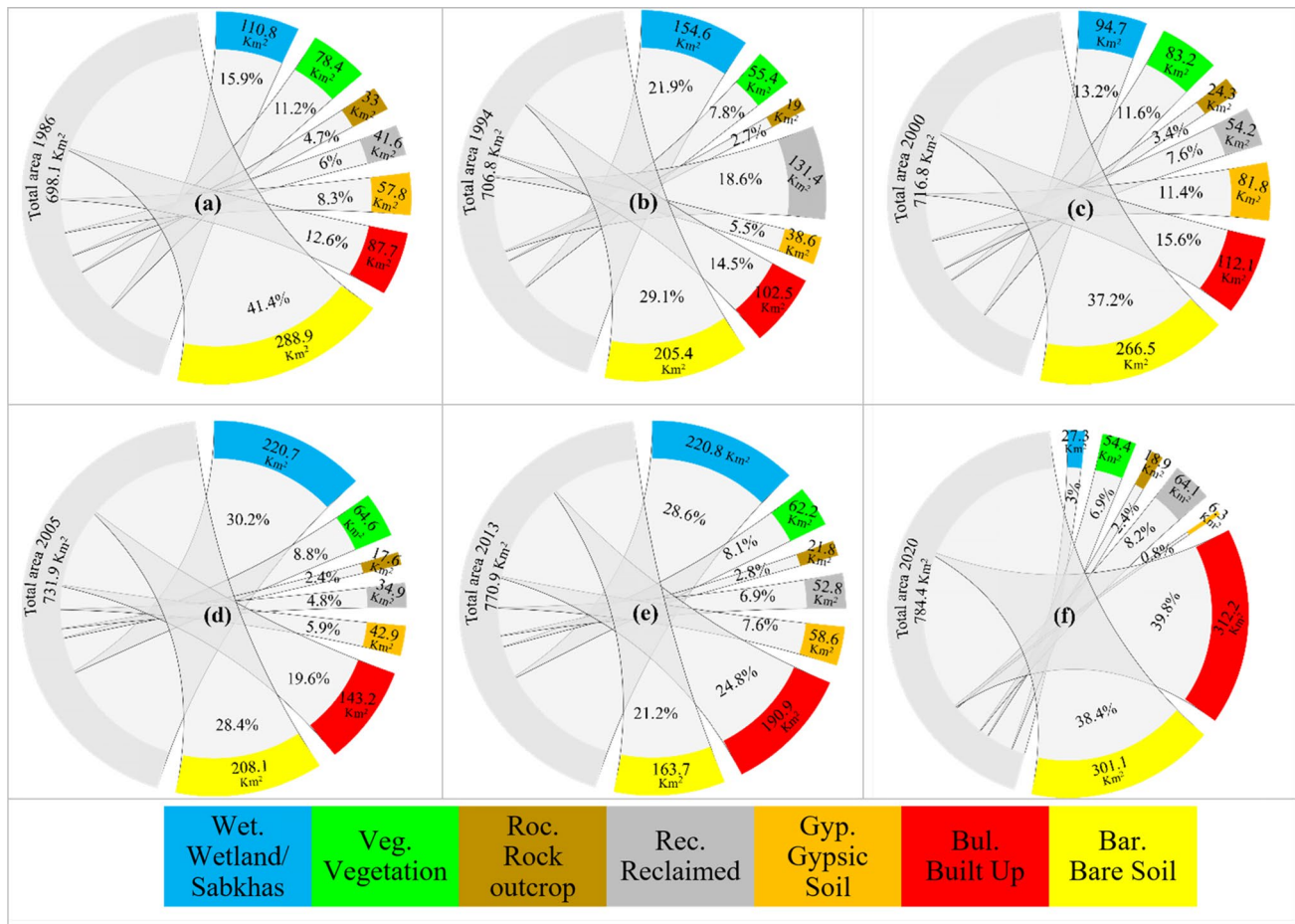


Fig. 4 Chord diagrams visualize the total area of LULC-classes and the total area, by km² for a 1986, b 1994, c 2000, d 2005, e 2013, and f 2020

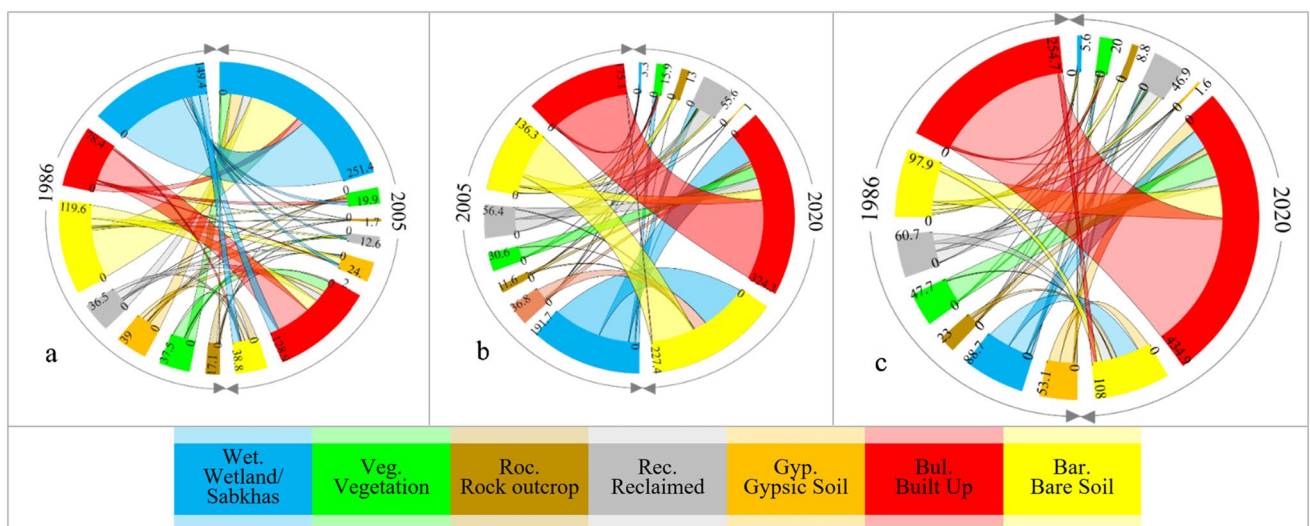


Fig. 5 a–c Chord diagrams explain the total area of LULC-classes transition by km² during for a 1986–2005, b 2005–2020, and c 1986–2020

4.2 LULC Classified Maps

The six classified raster maps were used to reach the objectives of LULC change detection in this study. Table 3, Fig. 3a–f, and chord diagram Fig. 4a–f explicate the result of the six classified raster maps of 1986, 1994, 2000, 2005, 2013, and 2020 in detail. The chord diagram represents flows (connections) between the seven classes of LULC (reclamation, vegetation, built-up, rock outcrop, bare soil, gypsic soil, and wetland/sabkhas). A fragment on the outer part of the circular layout represents each class in the chord diagram, and then arcs are drawn between each class. The size of the arc is proportional to the significance of the change. The results of the 1986 LULC classified image Fig. 3a shows that Bare soil dominates a total area (41.4%), followed by wetland and sabkhas (15.9%), as illustrated in Fig. 4a. The built-up area covered 12.6% of the total area. More than 78 km² of vegetation covered the ground, accounting for 11.2% of the total land surface. The rock outcrop takes up the minor land, accounting for only 4.7% of the total area. The 1994 LULC classified map results are demonstrated in Table 3, Figs. 3b, and 4b; the bare soil dominates a total area (29.1%), followed by wetland and sabkhas (21.9%), the built-up area covered 14.5% of the total area. More than 55.4 km² of vegetation covered the ground, accounting for 7.8% of the total land surface. The rock outcrop takes up a minor land area, accounting for only 2.7% of the total area. In 2000, the results of the classified image Figs. 3c and 4c indicated that the rock outcrop covers a minor part of the total area, which is 3.4% or 24.3 km². Bare soil covers a significant part of the total area, 37.2% (266.5 km²), whereas the wetland and sabkhas cover 13.2% (94.7 km²). The built-up area covers about (15.6%) 112.1 km² of the total area. The reclaimed area covers the smallest amount of land, accounting for only 7.6% of the total area. According to the classification results of 2005, Figs. 3d and 4d, wetland and sabkhas account for 30.2% of the total area or 220.7 km². Bare soil class accounts for 28.4% (208.1 km²) of the entire area. Nonetheless, the built-up area covers 19.6% (143.2 km²) of the land. Vegetation land covers 8.8% of the total land area (64.6 km²). The smallest class is the gypsic soils, which make up 5.9% of the total land area (42.9 km²). In the 2013 classified image results, Figs. 3e and 4e, the land area was covered by 28.6% wetland and sabkhas (220.8 km²), followed by built-up land (190.9 km², 24.8% of the total area). The bare soil covered 21.2% or 163.7 km². The reclaimed area covered 6.9% or 52.8 km² of the total area. The LULC classes for 2020, Fig. 3f, indicate that the built-up land and bare soil area almost occupied the same total area of 312.2 and 301.1 km², which account for 39.8% and 38.4% of the total area, respectively, Fig. 4f. On the other hand, the gypsic soils occupied the minor area this year and reached 0.8% or 6.3 km² of the total area.

4.3 LULC Change Detection

The spatial analysis was conducted to assess the patterns of LC-change and overall LU-changes from 1986 to 2020. The LULC-classes of the study area were reclaimed, vegetation, built-up, rock outcrop, bare land, gypsic soils, and wetland/sabkhas. We designated three critical years: the starting year of the study, 1986, the mid-year 2005 (approximately), and 2020. The change detection analysis concentrated on three periodic times by creating three area matrices from 1986–2005 and 2005–2020, and the whole period of the temporal study dates from 1986 to 2020. The changing patterns were depicted using chord diagrams. Table 4 illustrates the LULC classes in 1986, 2005, and 2020 for each class, the total area, and the spatio-temporal changes in the study area for the last 34 years. In addition, three chords' diagrams, Fig. 5a–c presents the changes from 1986–2005, 2005–2020, and 1986–2020. The total area of Bahrain has been increased by about 86 km² from 1986 to 2020. Dredging and reclaiming the islands' shallow water areas added nearly 33.8 and 52 km² to the total land area between 1986 and 2005 and 2005 and 2020. The LULC change detection for the last 34 years in Bahrain revealed that the "Built Up" areas increased, whereas gypsic soils, rock outcrop areas, wetland/Sabkhas, and vegetation decreased, Table 4. Comparing the statistics of 1986 and 2005 (19 years) reveals that there is a decline in reclaimed, vegetation, rock outcrop, bare soil, and gypsic soil areas by 66.6, 13.76, 15.47, 80.84, and 14.90 km², respectively, while there is an increase in built-up areas by 55.50 km². Between 2005 and 2020 (15 years), the changes indicate a decline in wetland/sabkhas, Gypsic soil, and vegetation areas by 193.40, 36.60, and 10.17 km², respectively. The built-up area has grown to reach 169.05 km². The changes in the last 34 years indicate that the built-up area is the most dominant category-class. From 1986 to 2020, the built-up area increased from 88 km² (12.6%) in 1986 to 224.54 km² (39.8%) of the total area of Bahrain land in 2020, respectively. The wetland/sabkhas, gypsic soils, vegetation, and rock outcrop have lost 83.41, 51.50, 23.93, and 14.11 km². The produced change maps and matrices were used to understand the changing status and magnitude rate for 1986–2005, 2005–2020, and 1986–2020.

Table 4 shows that four LULC classes have registered a negative annual change from 1986 to 2020. The vegetation, rock outcrop, gypsic soil, and wetland/sabkhas classes have recorded loss annually by -0.70 , -0.42 , -1.51 , and -2.45 km², respectively. The annual rate of change (ARC) of these classes were -1.59 , -0.90 , -1.26 , -2.26 , and -2.22% , respectively, for the same period. The built-up and bare soil gain was annually 6.6 and 0.36 km², respectively, and their annual rate of change was 7.49 and

0.12%, respectively. Built-up areas have registered the highest annual growth rate. The wetland/sabkhas registered the lowest annual growth rate in the last 34 years.

4.3.1 LULC Change Detection from 1986 to 2005

Table 5 and Fig. 5a depict LULC change transitions from 1986 to 2005. The LULC class is stated in terms of km². Most changes in the classes' category between 1986 and 2005 were in negative values except for built-up and wetland/sabkhas classes. The reclaimed areas converted mostly to wetland (14.1 km²). During this period, the vegetation class lost 13.8 km² and converted mainly to built-up. Furthermore, the rock outcrop class area lost 15.5 km², which converted to bare soil in 2005. 78.9 km² of the bare soil lands changed to wetlands in 2005, and 19.6 km² of the wetlands in 2005 were Gypsic soil in 1986. Moreover, 14.4 km² of the wetland in 1986 converted to built-up areas in 2005. Around 11.8 km² of the built-up area in 1986 became wetland areas in 2005 (reconstruction of new urban area). The chord diagram transitions are colorized to see how LULC-classes changed from 1986 to 2005. In 1986, the dominant classes were bare soils, wetland/sabkhas, and built-up areas, while in 2005, the bare soil area lost more than 80 km². The change detection from 1986 to 2005 indicates the shifting to the built-up area and reduction in vegetation land; however, the wetland/sabkhas were still the dominant class in 2005.

4.3.2 LULC Change Detection from 2005 to 2020

Table 5 and Fig. 5b describe the LULC-classes change transitions from 2005 to 2020. Three classes' category changes were negative, which means loss of wetland/sabkhas, Gypsic, and vegetation. The built-up, bare soils and reclamation classes increased in the area. Reclaimed areas have become mostly built-up areas; at least 25 km² from the reclaimed areas have been converted to built-up class. The vegetation class lost 10.2 km² and converted mainly to built-up. The rock-outcrop class area lost 6.30 km², which converted to bare soil in 2020. 25.8 km² of the bare soil lands were changed to built-up areas by 2020, 102.5 km² of the wetland in 2005 have converted to bare soil areas, and around 64.9 km² became built-up areas by 2020. The chord diagram visualizes the transitions of LULC-classes changes from 2005 to 2020. In 2005, the dominant classes were wetland/sabkhas, bare soils, and built-up areas. The chord diagram shows the reduction in vegetation land. The change detection from 2005 to 2020 indicates that the shifting to the built-up area has become dominant. Built-up area is equal to 20% of the country's total area in 2005.

4.4 LULC Change Detection from 1986 to 2020

Table 5 and Fig. 5c depict the LULC-classes change transitions from 1986 to 2020. Most changes in the classes' category between 1986 and 2020 were directed to built-up areas. The reclaimed areas were converted mostly to built-up and wetlands/sabkhas, and 18.2 and 18 km² were added to these classes. The vegetation class lost 43.6 km², which converted mainly to built-up areas. The rock outcrop class area lost 14.1 km², which converted mainly to bare soil in 2005. 60.8 km² of the bare soil areas changed to built-up by 2020. In addition, 23.9 and 34.4 km² from the gypsic soil wetland/sabkhas were added to built-up areas. 12.3 km² of the rock outcrop areas in 1986 converted to built-up areas by 2020. Around 83.4 km² of the wetland/sabkhas area in 1986 was lost. The change detection from 1986 to 2020 indicates the shifting of most LULC-classes to the built-up area and the reduction in vegetation and wetland/sabkhas land in the last 34 years. The change detection from 1986 to 2005 indicates the shifting to the built-up area and the reduction in vegetation land.

5 Conclusions

This study integrated remote sensing and GIS to quantify and analyze the LULC changes in Bahrain's main islands over 34 years from 1986 to 2020. Moreover, LULC changes between 1986, 2005, and 2020 were demonstrated and visualized using statistics and chord diagrams. Furthermore, the identified seven LULC-classes revealed substantial change patterns in the study area. LULC-changes were determined using six multitemporal Landsat satellite imagery, and the classification accuracy was measured using the confusion matrix. The overall classification accuracy was acceptable. Conferring to the quantitative evidence from our study, Bahrain Island has witnessed significant land use and land cover changes since 1986. The study results showed a significant change in the LULC during the study period. During the study period, the built-up areas showed an increasing trend of 7.5% annually, while the Gypsic, wetland/sabkhas, and vegetation showed a decreasing trend of 2.26, 2.22, and 0.9%, respectively. The changes in LULC were effectively captured by the remote sensing Landsat satellite sensors with different spectral, spatial, and temporal resolutions with GIS analysis. The change detection analysis using GIS and remote sensing delivers valuable information to understand the annual patterns of land use dynamics for planners and decision-makers; therefore, sustainable land management planning is possible. The expansion of the built-up area in the study area was mainly at the expense of vegetation and wetland/sabkhas lands. The results indicate that the built-up area covered more than 40% of Bahrain's main islands

land. For the environment's long-term sustainability, LULC changes should be constantly monitored in the future. Moreover, Landsat TM5, ETM+7, and OLI8 images archives and the newly invented remote sensing satellite imagery should be used to create and monitor accurate maps of LULC changes in Bahrain.

Supplementary Information The online version contains supplementary material available at <https://doi.org/10.1007/s41748-022-00315-z>.

Funding The authors have not disclosed any funding.

Declarations

Conflict of interest The corresponding author states that there is no conflict of interest on behalf of all the authors.

Open Access This article is licensed under a Creative Commons Attribution 4.0 International License, which permits use, sharing, adaptation, distribution and reproduction in any medium or format, as long as you give appropriate credit to the original author(s) and the source, provide a link to the Creative Commons licence, and indicate if changes were made. The images or other third party material in this article are included in the article's Creative Commons licence, unless indicated otherwise in a credit line to the material. If material is not included in the article's Creative Commons licence and your intended use is not permitted by statutory regulation or exceeds the permitted use, you will need to obtain permission directly from the copyright holder. To view a copy of this licence, visit <http://creativecommons.org/licenses/by/4.0/>.

References

- Adam E, Mutanga O, Odindi J, Abdel-Rahman EM (2014) Land-use/cover classification in a heterogeneous coastal landscape using RapidEye imagery: evaluating the performance of random forest and support vector machines classifiers. *Int J Remote Sens* 35(10):3440–3458
- Al-doski J, Mansor SB, Zuhaidi Mohd Shafri H (2013) Change detection process and techniques. *Civil Environ Res* 3(10):37–46
- Allen TR, Wang Y, Crawford TW (2013) Remote sensing of land cover dynamics. *Treatise on geomorphology*, vol 3. Elsevier, Amsterdam, pp 80–102
- Alrababah MA, Alhamad MN (2006) Land use/cover classification of arid and semi-arid Mediterranean landscapes using Landsat ETM. *Int J Remote Sens* 27(13):2703–2718
- Anderson JR, Hardy EE, Roach JT, Witmer RE (1976) A land use and land cover classification system for use with remote sensor data. U.S. *Geological Survey Professional Paper*, No. 964. USGS, Washington, D.C. <https://pubs.usgs.gov/pp/0964/report.pdf>
- Ayele GT, Tebeje AK, Demissie SS, Belete MA, Jemberrie MA, Teshome WM et al (2018) Time series land cover mapping and change detection analysis using geographic information system and remote sensing, Northern Ethiopia. *Air Soil Water Res* 11:1178622117751603
- Bekalo MT (2009) Spatial metrics and Landsat data for urban landuse change detection in Addis Ababa, Ethiopia (p. 89). Doctoral dissertation. <https://run.unl.pt/bitstream/10362/5403/1/TGEO0008.pdf>
- Berlanga-Robles CA, Ruiz-Luna A (2002) Land use mapping and change detection in the coastal zone of northwest Mexico using remote sensing techniques. *J Coastal Res* 18(3):514–522
- Bramhe VS, Ghosh SK, Garg PK (2018) Extraction of built-up areas using convolutional neural networks and transfer learning from sentinel-2 satellite images. *Int Arch Photogramm Remote Sens Spatial Inf Sci* 42(3):79–85
- Butt A, Shabbir R, Ahmad SS, Aziz N (2015) Land use change mapping and analysis using Remote Sensing and GIS: A case study of Simly watershed, Islamabad, Pakistan. *Egypt J Remote Sens Space Sci* 18(2):251–259
- Camargo FF, Sano EE, Almeida CM, Mura JC, Almeida T (2019) A comparative assessment of machine-learning techniques for land use and land cover classification of the Brazilian tropical savanna using ALOS-2/PALSAR-2 polarimetric images. *Remote Sens* 11(13):1600
- Campbell JB (2007) Introduction to remote sensing, 4th edn. The Guilford Press, New York
- Camps-Valls G, Benediktsson JA, Bruzzone L, Chanussot J (2011) Introduction to the issue on advances in remote sensing image processing. *IEEE J Sel Top Signal Process* 5(3):365–369
- Chander G, Markham BL, Helder DL (2009) Summary of current radiometric calibration coefficients for Landsat MSS, TM, ETM+, and EO-1 ALI sensors. *Remote Sens Environ* 113(5):893–903. <https://doi.org/10.1016/j.rse.2009.01.007>
- Chen T, Peng L, Wang Q, Liu S (2017) Measuring the coordinated development of ecological and economic systems in Hengduan Mountain area. *Sustainability* 9(8):1270. <https://doi.org/10.3390/su9081270>
- CIO. (1986–2013). Central Information Authority, Kingdom of the Navy. <http://www.cio.gov.bh/cioeng/default.aspx>
- Cohen WB, Goward SN (2004) Landsat's role in ecological applications of remote sensing. *Bioscience* 54(6):535–545
- Congalton RG (1991) A review of assessing the accuracy of classifications of remotely sensed data. *Remote Sens Environ*. [https://doi.org/10.1016/0034-4257\(91\)90048-B](https://doi.org/10.1016/0034-4257(91)90048-B)
- Congalton RG (2001) Accuracy assessment and validation of remotely sensed and other spatial information. *Int J Wildland Fire* 10(3–4):321–328. <https://doi.org/10.1071/wf01031>
- Congalton R, Green K (2019) Assessing the accuracy of remotely sensed data: principles and practices, 3rd edn. Taylor and Francis, London
- Da Costa SMF, Cintra JP (1999) Environmental analysis of metropolitan areas in Brazil. *ISPRS J Photogramm Remote Sens* 54(1):41–49
- DeMers MN (2008) Fundamentals of geographic information systems, 4th edn. Wiley, Hoboken
- Dewidar KM (2004) Detection of land use/land cover changes for the northern part of the Nile delta (Burullus region), Egypt. *Int J Remote Sens* 25(20):4079–4089
- Dobson MC, Ulaby FT, Pierce LE (1995) Land-cover classification and estimation of terrain attributes using synthetic aperture radar. *Remote Sens Environ* 51(1):199–214. [https://doi.org/10.1016/0034-4257\(94\)00075-X](https://doi.org/10.1016/0034-4257(94)00075-X)
- Duan Y, Wang X, Wei Y (2020) Land use change analysis of Daishan Island using multi-temporal remote sensing imagery. *Arab J Geosci* 13:741. <https://doi.org/10.1007/s12517-020-05513-5>
- El-Hattab MM (2016) Applying post classification change detection technique to monitor an Egyptian coastal zone (Abu Qir Bay). *Egypt J Remote Sens Space Sci* 19(1):23–36
- Epstein J, Payne K, Kramer E (2002) Techniques for mapping suburban sprawl. *Photogramm Eng Remote Sens* 68(9):913–918
- EROS (2021) Earth Resources Observation and Science (EROS) Center. <https://www.usgs.gov/centers/eros/data>
- Feng D, Yu L, Zhao Y, Cheng Y, Xu Y, Li C, Gong P (2018) A multiple dataset approach for 30-m resolution land cover

- mapping: a case study of continental Africa. *Int J Remote Sens* 39(12):3926–3938. <https://doi.org/10.1080/01431161.2018.1452073>
- Ferrara A, Biró M, Malatesta L, Molnár Z, Mugnoz S, Tardella FM, Catorci A (2021) Land-use modifications and ecological implications over the past 160 years in the central Apennine mountains. *Landsc Res*. <https://doi.org/10.1080/01426397.2021.1922997>
- Ferrari A, Russo M (2016) *Introducing Microsoft power BI*. Microsoft Press, Washington
- Footy GM (2002) Status of land cover classification accuracy assessment. *Remote Sens Environ* 80(1):185–201
- Forget Y, Linard C, Gilbert M (2017) Automated supervised classification of Ouagadougou built-up areas in Landsat scenes using OpenStreetMap. In *2017 Joint Urban Remote Sensing Event (JURSE)*, pp. 1–4. IEEE. <https://ieeexplore.ieee.org/abstract/document/7924571>
- Franklin J (1995) Predictive vegetation mapping: geographic modelling of biospatial patterns in relation to environmental gradients. *Prog Phys Geogr* 19(4):474–499
- Gallego FJ (2004) Remote sensing and land cover area estimation. *Int J Remote Sens* 25(15):3019–3047. <https://doi.org/10.1080/01431160310001619607>
- Ghosh S, Siddique G (2018) Change detection of built up areas applying built-up index for Chandannagar city. *Int J Technol Res Manag* 5(4):1–7
- Green L, Fry AF, Myerson J (1994) Discounting of delayed rewards: a life-span comparison. *Psychol Sci* 5(1):33–36. <https://doi.org/10.1111/j.1467-9280.1994.tb00610.x>
- Guerschman JP, Paruelo JM, Bella CD, Giallorenzi MC, Pacin F (2003) Land cover classification in the Argentine Pampas using multi-temporal Landsat TM data. *Int J Remote Sens* 24(17):3381–3402. <https://doi.org/10.1080/0143116021000021288>
- Haque MI, Basak R (2017) Land cover change detection using GIS and remote sensing techniques: a spatio-temporal study on Tanguar Haor, Sunamganj, Bangladesh. *Egypt J Remote Sens Space Sci* 20(2):251–263. <https://doi.org/10.1016/j.ejrs.2016.12.003>
- Harris PM, Ventura SJ (1995) The integration of geographic data with remotely sensed imagery to improve classification in an urban area. *Photogramm Eng Remote Sens* 61(8):993–998
- Hegazy IR, Kaloop MR (2015) Monitoring urban growth and land use change detection with GIS and remote sensing techniques in Daqahlia governorate Egypt. *Int J Sustain Built Environ* 4(1):117–124. <https://doi.org/10.1016/j.ijsbe.2015.02.005>
- Hurskainen P, Adhikari H, Siljander M, Pellikka PKE, Hemp A (2019) Auxiliary datasets improve accuracy of object-based land use/land cover classification in heterogeneous savanna landscapes. *Remote Sens Environ* 233:111354. <https://doi.org/10.1016/j.rse.2019.111354>
- Information and eGovernment Authority (2018) Bahrain open data portal. Central Organization Statistics. <https://www.iga.gov.bh/en/>
- Information and eGovernment Authority (2020) Bahrain open data portal. Central Organization Statistics. <https://www.iga.gov.bh/en/>
- Islam K, Jashimuddin M, Nath B, Nath TK (2018) Land use classification and change detection by using multi-temporal remotely sensed imagery: The case of Chunati wildlife sanctuary, Bangladesh. *Egypt J Remote Sens Space Sci* 21(1):37–47. <https://doi.org/10.1016/j.ejrs.2016.12.005>
- Jacquin A, Misakova L, Gay M (2008) A hybrid object-based classification approach for mapping urban sprawl in periurban environment. *Landsc Urban Plan* 84(2):152–165. <https://doi.org/10.1016/j.landurbplan.2007.07.006>
- Jamali A (2019) Evaluation and comparison of eight machine learning models in land use/land cover mapping using Landsat 8 OLI: a case study of the northern region of Iran. *SN Appl Sci* 1(11):1–11
- Jansen LJM, Di Gregorio A (2004) Obtaining land-use information from a remotely sensed land cover map: results from a case study in Lebanon. *Int J Appl Earth Obs Geoinf* 5(2):141–157. <https://doi.org/10.1016/j.jag.2004.02.001>
- Jensen JR (1996) *Introductory digital image processing: a remote sensing perspective*, 2nd edn. Prentice Hall, Upper Saddle River
- Jensen JR (2005) *Introductory digital image processing: a remote sensing perspective*, 3rd edn. Prentice Hall, Upper Saddle River
- Jensen JR, Cowen DC (1999) Remote sensing of urban/suburban infrastructure and socio-economic attributes. *Photogramm Eng Remote Sens* 65:611–622
- Kacem HA, Maan M, Rhinane H (2021) The value of carbon sequestration and storage in coastal habitats areas in North West of Morocco. In *E3S Web of Conferences*, vol. 240. EDP Sciences. <https://doi.org/10.1051/e3sconf/202124001003>
- Keshkar H, Voigt W (2016) A spatiotemporal analysis of landscape change using an integrated Markov chain and cellular automata models. *Model Earth Syst Environ* 2(1):1–13
- Koc D, Ikiel C, Atalay A, Ustaoglu B (2012) Land use and land cover (LULC) classification using spot-5 image in the Adapazari plain and its surroundings, Turkey. *Online J Sci Technol* 2:37–42
- Lillesand TM, Kiefer RW (1999) *Remote sensing and image interpretation*, 4th edn. Wiley, Hoboken
- Lillesand T, Kiefer RW, Chipman J (2015) *Remote sensing and image interpretation*, 7th edn. Wiley, Hoboken
- Lu D, Weng Q (2009) Extraction of urban impervious surfaces from an IKONOS image. *Int J Remote Sens* 30(5):1297–1311
- Lu D, Mausel P, Brondizio E, Moran E (2004) Change detection techniques. *Int J Remote Sens* 25(12):2365–2401. <https://doi.org/10.1080/0143116031000139863>
- Lu D, Hetrick S, Moran E (2010) Land cover classification in a complex urban-rural landscape with QuickBird imagery. *Photogramm Eng Remote Sens* 76(10):1159–1168
- Ma L, Liu Y, Zhang X, Ye Y, Yin G, Johnson BA (2019) Deep learning in remote sensing applications: a meta-analysis and review. *ISPRS J Photogramm Remote Sens* 152:166–177
- Macleod RD, Congalton RG (1998) A quantitative comparison of change-detection algorithms for monitoring eelgrass from remotely sensed data. *Photogramm Eng Remote Sens* 64(3):207–216
- Manandhar R, Odeh IO, Ancev T (2009) Improving the accuracy of land use and land cover classification of Landsat data using post-classification enhancement. *Remote Sens* 1(3):330–344
- Matlhodi B, Kenabatho PK, Parida BP, Maphanyane JG (2019) Evaluating land use and land cover change in the Gaborone dam catchment, Botswana, from 1984–2015 using GIS and remote sensing. *Sustainability* 11(19):5174. <https://doi.org/10.3390/su11195174>
- Maxwell AE, Warner TA, Fang F (2018) Implementation of machine-learning classification in remote sensing: an applied review. *Int J Remote Sens* 39(9):2784–2817
- Mesaier ARA, Al-Zayani AK (2008) *The environment in the Kingdom of Bahrain is real and challenging*, 1st edn. Bahrain Centre for Studies and Research, Manama Kingdom (**In Arabic**)
- Mollicone D, Achard F, Eva H, Belward AS, Federici S, Lumericis A, et al. (2003) Land use change monitoring in the Framework of the UNFCCC and its Kyoto Protocol: report on current capabilities of satellite remote sensing technology. European Communities, Luxembourg. EUR, 20867
- Ndehedehe CE, Oludiji SM, Asuquo IM (2013) Supervised learning methods in the mapping of built up areas from Landsat-based satellite imagery in part of Uyo Metropolis. *N Y Sci J* 6(9):45–52
- Petit CC, Lambin EF (2001) Integration of multi-source remote sensing data for land cover change detection. *Int J Geogr Inf Sci* 15(8):785–803. <https://doi.org/10.1080/13658810110074483>

- Rawat JS, Kumar M (2015) Monitoring land use/cover change using remote sensing and GIS techniques: a case study of Hawalbagh block, district Almora, Uttarakhand, India. *Egypt J Remote Sens Space Sci* 18(1):77–84. <https://doi.org/10.1016/j.ejrs.2015.02.002>
- Rogan J, Chen D (2004) Remote sensing technology for mapping and monitoring land-cover and land-use change. *Prog Plan* 61(4):301–325
- Roy A, Inamdar AB (2019) Multi-temporal Land Use Land Cover (LULC) change analysis of a dry semi-arid river basin in western India following a robust multi-sensor satellite image calibration strategy. *Heliyon* 5(4):e01478. <https://doi.org/10.1016/j.heliyon.2019.e01478>
- Shih HC, Stow DA, Tsai YH (2019) Guidance on and comparison of machine learning classifiers for Landsat-based land cover and land use mapping. *Int J Remote Sens* 40(4):1248–1274
- Siddique MA, Dongyun L, Li P, Rasool U, Khan TU, Farooqi TJA et al (2020) Assessment and simulation of land use and land cover change impacts on the land surface temperature of Chaoyang District in Beijing, China. *PeerJ* 8:e9115. <https://doi.org/10.7717/peerj.9115>
- Singh A (1989) Review article digital change detection techniques using remotely sensed data. *Int J Remote Sens* 10(6):989–1003
- Talukdar S, Singha P, Mahato S, Praveen B, Rahman A (2020) Dynamics of ecosystem services (ESs) in response to land use land cover (LU/LC) changes in the lower Gangetic plain of India. *Ecol Ind* 112:106121
- Tena TM, Mwaanga P, Nguvulu A (2019) Impact of land use/land cover change on hydrological components in Chongwe River Catchment. *Sustainability* 11(22):6415. <https://doi.org/10.3390/su11226415>
- Tewabe D, Fentahun T (2020) Assessing land use and land cover change detection using remote sensing in the Lake Tana Basin, Northwest Ethiopia. *Cogent Environ Sci* 6(1):1778998. <https://doi.org/10.1080/23311843.2020.1778998>
- Ukor CD, Ogbole J, Alaga A (2016) Analysis of land use land cover change in Ikeja, Lagos State, Nigeria using remote sensing and Gis techniques. *Int J Sci Technol* 5(10):462–472
- Ulbricht KA, Heckendorff WD (1998) Satellite images for recognition of landscape and landuse changes. *ISPRS J Photogramm Remote Sens* 53(4):235–243. [https://doi.org/10.1016/S0924-2716\(98\)00006-9](https://doi.org/10.1016/S0924-2716(98)00006-9)
- UNdata (2021) A world of information. Popular Statistical Table, Country (Area) and Regional Profiles. 2 Population, Surface Area and Density. United Nations Statistics Division. http://data.un.org/_Docs/SYB/PDFs/SYB64_1_202110_Population,%20Surface%20Area%20and%20Density.pdf. Accessed 3 January 2022
- UNDP (2018) Bahrain Human Development Report 2018: Pathways to Sustainable Economic Growth in Bahrain. United Nations Development Programme 2021. https://www.bh.undp.org/content/bahrain/en/home/library/human_development/Bahrain_Human_Development_Report_2018.html
- UPDA (2022) A New Strategy for a Brighter Future. Urban Planning and Development Authority. Kingdom of Bahrain. <https://upda.gov.bh/en/category/map-of-bahrain-national-detail-land-use-plan>, https://upda.gov.bh/Media/ZonningMappings/20190908083120093_tpb0a222_qfj.pdf, <https://www.arcgis.com/apps/webappviewer/index.html?id=b4f12e4d504b4f7daa4ed7743548d71a>, <https://upda.gov.bh/en/category/capital-governorate>
- Viana CM, Rocha J (2020) Evaluating dominant land use/land cover changes and predicting future scenario in a rural region using a memoryless stochastic method. *Sustainability* 12(10):4332. <https://doi.org/10.3390/su12104332>
- Vigneshwaran S, Kumar SV (2018) Extraction of built-up area using high resolution sentinel-2a and google satellite imagery. *International Archives of the Photogrammetry, Remote Sensing & Spatial Information Sciences*, 42. <https://pdfs.semanticscholar.org/a456/f6308b936312b1fc42b99e92d81751ef5946.pdf>
- Vinatier F, Arnaiz AG (2018) Using high-resolution multitemporal imagery to highlight severe land management changes in Mediterranean vineyards. *Appl Geogr* 90:115–122. <https://doi.org/10.1016/j.apgeog.2017.12.003>
- Wang SW, Gebru BM, Lamchin M, Kayastha RB, Lee WK (2020) Land use and land cover change detection and prediction in the Kathmandu district of Nepal using remote sensing and GIS. *Sustainability* 12(9):3925. <https://doi.org/10.3390/su12093925>
- Weng Q (2002) Land-use change analysis in the Zhujiang Delta of China using satellite remote sensing, GIS, and stochastic modeling. *J Environ Manage* 64(3):273–284
- Wu Q, Li H, Wang R, Paulussen J, He Y, Wang M, Wang B, Wang Z (2006) Monitoring and predicting land use change in Beijing using remote sensing and GIS. *Landsat Urban Plan* 78(4):322–333. <https://doi.org/10.1016/j.landurbplan.2005.10.002>
- Wulder MA, White JC, Goward SN, Masek JG, Irons JR, Herold M, Cohen WB, Loveland TR, Woodcock CE (2008) Landsat continuity: Issues and opportunities for land cover monitoring. *Remote Sens Environ* 112(3):955–969. <https://doi.org/10.1016/j.rse.2007.07.004>
- Xiao J, Shen Y, Ge J, Tateishi R, Tang C, Liang Y, Huang Z (2006) Evaluating urban expansion and land use change in Shijiazhuang, China, by using GIS and remote sensing. *Landsat Urban Plan* 75(1–2):69–80. <https://doi.org/10.1016/j.landurbplan.2004.12.005>
- Xiao D, Niu H, Guo J, Zhao S, Fan L (2021) Carbon storage change analysis and emission reduction suggestions under land use transition: a case study of Henan Province, China. *Int J Environ Res Public Health* 18(4):1844. <https://doi.org/10.3390/ijerph18041844>
- Xu H (2007) Extraction of urban built-up land features from Landsat imagery using a thematic oriented index combination technique. *Photogramm Eng Remote Sens* 73(12):1381–1391
- Xu L, Zhang S, He Z, Guo Y (2009) The comparative study of three methods of remote sensing image change detection. In 2009 17th International Conference on Geoinformatics, 1–4. IEEE.
- Yu L, Wang J, Gong P (2013) Improving 30 m global land-cover map FROM-GLC with time series MODIS and auxiliary data sets: a segmentation-based approach. *Int J Remote Sens* 34(16):5851–5867
- Yuan F, Sawaya KE, Loeffelholz BC, Bauer ME (2005) Land cover classification and change analysis of the Twin Cities (Minnesota) Metropolitan Area by multitemporal Landsat remote sensing. *Remote Sens Environ* 98(2–3):317–328
- Zanotta DC, Zortea M, Ferreira MP (2018) A supervised approach for simultaneous segmentation and classification of remote sensing images. *ISPRS J Photogramm Remote Sens* 142:162–173
- Zha Y, Gao J, Ni S (2003) Use of normalized difference built-up index in automatically mapping urban areas from TM imagery. *Int J Remote Sens* 24(3):583–594
- Zhang J, Li P, Wang J (2014) Urban built-up area extraction from Landsat TM/ETM+ images using spectral information and multivariate texture. *Remote Sens* 6:7339–7359. <https://doi.org/10.3390/rs6087339>
- Zhu Z, Gallant AL, Woodcock CE, Pengra B, Olofsson P, Loveland TR, Jin S, Dahal D, Yang L, Auch RF (2016) Optimizing selection of training and auxiliary data for operational land cover classification for the LCMAP initiative. *ISPRS J Photogramm Remote Sens* 122:206–221. <https://doi.org/10.1016/j.isprsjprs.2016.11.004>
- Zougrana BJ, Conrad C, Amekudzi LK, Thiel M, Da ED, Forkuor G, Löw F (2015) Multi-temporal Landsat images and ancillary data for land use/cover change (LULCC) detection in the Southwest of Burkina Faso, West Africa. *Remote Sens* 7(9):12076–12102
- Zsuzsanna D, Bartholy J, Pongracz R, Barcza Z (2005) Analysis of land-use/land-cover change in the Carpathian region based on remote sensing techniques. *Phys Chem Earth* 30:109–115